



## ISTITUTO NAZIONALE DI RICERCA METROLOGICA Repository Istituzionale

Metrological setup for accurate determination of passive radiative cooling power

*Original*

Metrological setup for accurate determination of passive radiative cooling power / Lopardo, G.; Bertiglia, F.; Braccialarghe, G.; Florio, M.; Girard, F.; Giraudi, D.; Santoro, F.; Pattelli, L.. - In: APPLIED THERMAL ENGINEERING. - ISSN 1359-4311. - 292:(2026). [10.1016/j.applthermaleng.2026.130363]

*Availability:*

This version is available at: 11696/88066 since: 2026-02-24T16:00:43Z

*Publisher:*

Elsevier

*Published*

DOI:10.1016/j.applthermaleng.2026.130363

*Terms of use:*

This article is made available under terms and conditions as specified in the corresponding bibliographic description in the repository

*Publisher copyright*

(Article begins on next page)



## Research Paper

# Metrological setup for accurate determination of passive radiative cooling power

G. Lopardo<sup>\*</sup>, F. Bertiglia, G. Braccialarghe, M. Florio, F. Girard, D. Giraudi, F. Santoro, L. Pattelli

Istituto Nazionale di Ricerca Metrologica – INRiM, Strada Delle Cacce, 91, 10135 Turin, Italy

## ARTICLE INFO

## Keywords:

Passive radiative cooling  
Radiative heat transfer  
Cooling power density  
Temperature measuring device  
Uncertainty evaluation  
Thermopile

## ABSTRACT

Passive radiative cooling (PRC) enables heat rejection to the cold sky through the atmospheric transparency window and has attracted increasing attention as a power-free cooling strategy. However, reported cooling performances remain difficult to compare and often unreliable, primarily due to the lack of metrologically sound measurement methods and quantitative uncertainty assessment.

In this work, a fluid-based calorimetric apparatus is designed according to a traceable metrological framework for the accurate determination of PRC cooling power. The system offers a compact panel-like geometry with uniform liquid flow distribution and employs high-sensitivity, SI-traceable sensors. In particular, the temperature difference between inlet and outlet water is measured directly using a calibrated multi junction differential thermocouple (thermopile) achieving an expanded uncertainty of just 12.4 mK, allowing to reliably measure also small temperature differences between the panel outlet and inlet ports. Together with a calibrated flow-rate measurement and a full uncertainty budget, the proposed design allows relative uncertainties consistently below 10% over almost the complete range of power densities relevant to PRC materials. Even at moderate fluxes, and in the presence of non-radiative heat transfer contributions, the setup achieves a significant improvement over the measurement uncertainties reported in the literature for comparable setups.

These results and comparative analysis demonstrate that metrology-driven design is essential for reliable PRC performance assessment and provide a robust benchmark for future material development and system-level studies.

## 1. Introduction

The World Meteorological Organization certified 2024 as the warmest year on record [1], smashing the previous 2023 record, and marking a point of no return as the first year to exceed 1.5 °C above pre-industrial levels [2]. Accelerating global warming is expected to drive cooling needs to new extremes which are unsustainable in terms of costs, electric grid capacity, CO<sub>2</sub> emissions and leakages of refrigerant gases. To address this multi-faceted issue, passive radiative cooling (PRC) materials represent a new, sustainable and low-cost cooling strategy that does not rely on vapor compression.

Enabled by advances in materials engineering, PRC emitters with tailored emissivity in the thermal infrared range can reject their heat to outer space through the atmospheric transparency window (8–13 μm). While radiative cooling has long been exploited during nighttime conditions, recent developments have demonstrated net cooling even under

direct solar illumination by combining high infrared emissivity with solar reflectivity [3].

Following these initial breakthroughs, a rapidly growing body of literature has explored potential applications of passive radiative cooling. These can be broadly classified into passive implementations, where radiative cooling materials are directly applied to the object to be cooled—such as photovoltaic modules [4,5], building envelopes and cool roofs [6,7], or even the human body [8,9]—and active implementations, where radiative cooling is used to generate cooled heat-transfer fluids (e.g., water) that can be coupled to external thermal systems, including vapor-compression refrigeration units [10,11], power plant condensers [12,13], and other infrastructures. Active approaches are particularly attractive because the cooling effect can be modulated, stored, and dispatched on demand via fluid circulation, facilitating integration into realistic energy systems.

Irrespective of the application, accurately assessing the cooling

<sup>\*</sup> Corresponding author.

E-mail address: [g.loparto@inrim.it](mailto:g.loparto@inrim.it) (G. Lopardo).

performance of PRC materials under their intended operating conditions remains challenging. Reliable performance evaluation requires outdoor deployment with direct sky access and careful separation of radiative effects from parasitic heat-transfer pathways. To date, experiments are typically performed considering a couple of main figures of merit [14–16], namely the stagnation temperature reached when the net radiative flux vanishes, or the indirect estimation of cooling power density via Joule heating required to maintain the emitter at ambient temperature.

Unfortunately, in-field testing of PRC materials is often implemented with insufficient metrological rigor, leading to questionable claims of cooling performance observed using low-quality materials or inadequately controlled testing configurations—a concern that has been critically highlighted by several authors [17–19]. This situation underscores the need for more reliable and comparable measurement methodologies, including proper sensor calibration, uncertainty evaluation, and traceability to the International System of Units (SI).

Beyond accurate ambient temperature measurements [18,19], several additional factors critically affect the absolute accuracy of PRC performance assessment. Especially under daytime conditions, sub-ambient cooling effects are inevitably modest and typically limited to just a few degrees or less. In this regime, sensor calibration, positioning and uncertainty become decisive, as even small systematic biases can dominate the measured signal. Moreover, repeating measurements to assess reproducibility is inherently difficult due to continuously varying environmental conditions. As a result, temperature differences and inferred cooling powers are typically reported in the literature without quantified uncertainty or systematic error analysis. Similar limitations apply to Joule-heating-based approaches. While forcing the emitter at ambient temperature reduces convection and conduction contributions, many experimental designs assume purely one-dimensional heat transfer and neglect lateral losses, which can lead to overestimation of the radiative cooling power.

Based on these considerations, precise evaluation of PRC performance requires a measurement setup capable of isolating heat fluxes while minimizing interference from other heat-transfer pathways. In response to this need, we designed a fluid-based calorimetric apparatus with a focus on metrological principles, aiming to realize a consistent assessment of cooling performance. The sensors employed are calibrated against National references, which allows to obtain accurate and traceable measurements with a well-defined uncertainty budget.

This paper illustrates the advantages of the proposed design compared with existing measurement approaches reported in the literature, and discusses the strategies adopted to minimize systematic biases and overestimation of radiative fluxes. An overall uncertainty budget for cooling power is established, accounting for contributions from temperature and flow-rate measurements as well as typical non-radiative interference terms. This analysis highlights (i) an intrinsic uncertainty limitation affecting commonly used discrete thermistors approaches, which is overcome here by direct differential measurement, and (ii) the benefit from a compact form factor, which promotes more homogeneous heat exchange and reduced susceptibility to non-radiative parasitic effects.

The operating principle and realization details of the device are presented in Section 2, with a discussion on how to minimize non-radiative contributions. In Section 3, measurement uncertainty is estimated over the parameter space relevant to PRC characterization, including a systematic comparison with representative calorimetric setup from the literature. Finally, conclusions and outlook are given in Section 4.

## 2. Measurement principle and apparatus design

The underlying measurement principle of the apparatus is based on calorimetry—a classical technique for quantifying heat transfer via thermal energy balance. Specifically, a temperature-controlled working

fluid (water) circulates beneath a planar PRC-coated surface, and the net heat exchanged by the surface is inferred from the flow rate and the temperature difference between the fluid inlet and outlet. Under the assumption of negligible conduction and convection contributions, this thermal energy exchange can be attributed primarily to radiation.

Considering the difficulty in estimating the various coefficients appearing in the heat transfer equations for conduction and convection, the best way to make such contributions negligible is by minimizing the temperature difference between the PRC material and its surrounding ambient. The optimal strategy is to keep the mean working fluid temperature (average of inlet and outlet) to ambient temperature.

In this framework, the radiative heat power density,  $q$ , is given by the relation:

$$q = \frac{\dot{m}c_p\Delta T}{A}$$

where  $A$  is the emitter area,  $c_p$  is the (water) specific heat capacity,  $\dot{m}$  is the mass flow rate, and  $\Delta T = T_{\text{in}} - T_{\text{out}}$  is the measured water temperature drop across the panel. The mass flow rate,  $\dot{m}$ , is obtained from the volumetric flow rate  $Q$  as  $\dot{m} \approx \rho \cdot \dot{V} = \rho Q / 3600$ , with  $\rho \approx 1 \text{ kg}\cdot\text{L}^{-1}$  and  $Q$  expressed in L/h. Under these conditions, the expected temperature drop across the panel surface is therefore:

$$\Delta T(q, Q) = \frac{qA}{\dot{m}c_p}$$

which can be used to build the operating parameter landscape of the experimental setup.

A schematic representation of the working principle of the envisioned experimental setup realized is given in Fig. 1A. The apparatus consists of a water vessel sealed by an aluminium plate where the PRC material under study is applied. Working with a thermal mass (water) under the panel offers several advantages over existing solutions with thermometers bonded under the PRC plate. First, it resolves the critical issue of optimal thermal contact between the sample and the temperature sensor, which can be directly immersed in the heat exchange fluid wetting the back-surface of the emitter. By doing so, the thermal contact and consequently the heat exchange between the plate supporting the PRC sample and the sensing thermometers is more efficient and reproducible. Optimally, the outlet aperture can be slightly elevated with respect to the inlet, to ensure that a possible micro-bubble transported with the water flow can leave the vessel easily. Secondly, its panel-like configuration constitutes one of the main envisioned embodiments of this technology in practical applications [20–22], thus streamlining the study of its dependence on parameters such as inlet fluid temperature or flux [10].

The water flow rate under the PRC materials is constantly measured using a flow meter (model AF-E 400, Krohne) calibrated against Italian National standards.

The water temperature is regulated by a thermostatic circulation bath (model HAAKE G50 Thermo Scientific), which can be used to condition water temperature at a given position in the system, where water temperature is measured. Details about the thermal sensors and their arrangement inside the panel are provided in the next Subsection.

The experimental setup allows to work in two measurement configurations:

1. In static configuration, with still water under the sample, it is possible to measure the temperature drop between the PRC and the ambient using a series of discrete thermometers located at different positions under the panel.
2. In dynamic configuration, with flowing water, it is possible to evaluate the cooling power of the PRC material using a thermopile for measuring temperature difference between inlet and outlet.

Using the second measurement configuration, it is possible to

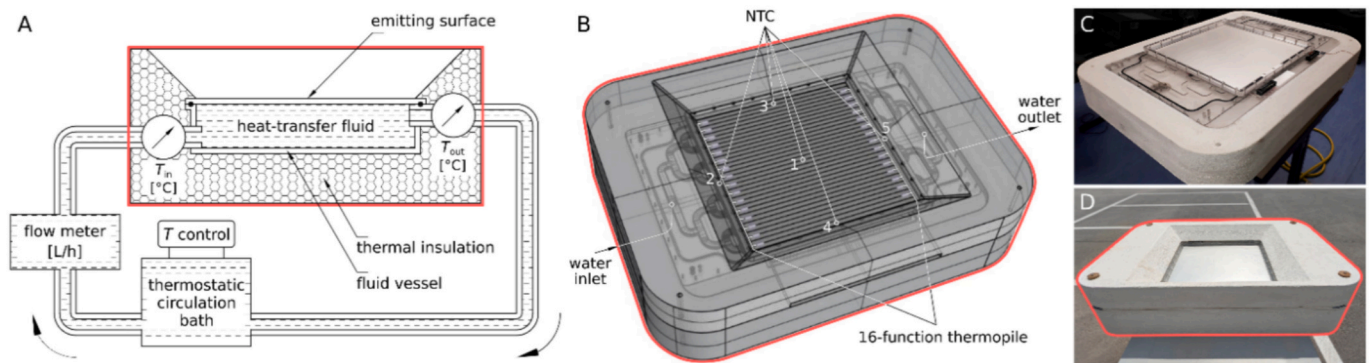


**Fig. 1.** (A) Schematic representation of the experimental setup. (B) Technical drawing indicating channel layout and sensor positions. (C–D) Photographs of the assembled test rig, showing, without and with the upper insulation cover.

overcome the difficulties related to the accurate evaluation of the non-radiative heat transfer coefficient [15,23]. In fact, a direct measurement of the cooling power, rather than of temperature drop, allows to minimize conduction and convection processes, which are always present in case of temperature differences between the PRC sample and the surrounding environment.

### 2.1. Test panel and structural design

The water vessel consists of a low thermal conductivity PMMA (polymethyl methacrylate, thermal conductivity typically between  $0.19$  and  $0.25 \text{ W}\cdot\text{m}^{-1}\cdot\text{K}^{-1}$ ), precision-machined with 32 longitudinal channels to allow fluid flow. The channels, having a cross section of  $14 \text{ mm} \times 3 \text{ mm}$ , are spaced by  $1 \text{ mm}$  thick ridges, which act both as structural supports for the aluminium substrate where the PRC material is applied and minimal thermal contact points.

The shallow channel depth ( $3 \text{ mm}$ ) and forced circulation also limit vertical stratification, ensuring that  $\approx 94\%$  of back surface of PRC sample is in direct contact with water.

The clear PMMA material conveniently allows visual inspection of the fluid flow inside the vessel for diagnostic purposes. Fig. 1B illustrates the device in a technical drawing and in its fully assembled form (C–D).

Water enters the system through the bottom surface into a main channel, which subsequently splits into two smaller channels. These channels then split again, continuing the division in a binary tree structure until the 32 identical channels are formed, as shown in Fig. 1B. This particular inlet configuration allows an equal partitioning of the water in the channels. The same layout is present at the outlet.

This design enforces equal channel partitioning and strongly reduces preferential paths and stagnant regions that can otherwise produce spurious temperature gradients, which were found to be a limitation or even provide thermal short-cuts in previously published designs [20]. The uniformity of the water flow, favoured also by the compact panel size, is essential to guaranteeing good thermal contact between temperature sensors and the PRC sample.

The aluminium test panel (thickness of  $0.8 \text{ mm}$ ) has a double utility: it seals the vessel ensuring mechanical integrity to the PRC samples and enhances thermal contact between the PRC material and the heat exchange fluid. In fact, PRC materials, which are commonly available as self-adhesive films, paints or membranes, lack sufficient inherent stiffness and require bonding to a supporting substrate for stability and consistent testing. To avoid mechanical deformation of the thin aluminium panel while ensuring hydraulic integrity, the system is operated with a negative gauge pressure at the outlet rather than a positive pressure from the inlet. This choice minimizes risk of panel buckling while preserving uniform channel flow distribution. Finally, the aluminium plates are interchangeable, allowing to test different PRC materials.

The panel size is  $50 \text{ cm} \times 50 \text{ cm}$  (exposed area:  $48 \text{ cm} \times 48 \text{ cm}$ ),

offering a good compromise between heat flux measurement resolution and manageability.

The entire assembly is enclosed in a box of high-density expanded polystyrene foam (HD-EPS,  $\approx 23 \text{ kg}\cdot\text{m}^{-3}$ ), with  $10 \text{ cm}$  thick walls to shield it from solar light and reduce non-radiative heat-exchange with the environment (Figs. 1C–D). As a thermally insulating material, HD-EPS offers several advantages: low thermal conductivity ( $0.031\text{--}0.035 \text{ W}\cdot\text{m}^{-1}\cdot\text{K}^{-1}$ ), high manufacturability, long-term stability and limited moisture uptake thanks to its closed-cell structure.

### 2.2. Thermal control

The location of thermal sensors is shown schematically in Fig. 1B.

A key innovation of the system is the use of a differential multi-junction type-T thermocouple (thermopile) for measuring the fluid temperature difference between inlet and outlet. Thermocouple junctions are positioned alternately every two channels. This configuration produces an amplified voltage response—approximately 16 times higher than a standard single-junction thermocouple—enabling exceptional sensitivity.

The thermopile, connected to a  $6\frac{1}{2}$ -digit multimeter (model 2700, Keithley), was characterized in a thermostatic bath in order to determine its sensitivity ( $657.7 \mu\text{V}/^\circ\text{C}$  near ambient temperature) and to assess any offsets induced by parasitic electromotive forces arising from imperfections in the wiring. The expanded temperature uncertainty for the thermopile is  $12.4 \text{ mK}$ , accounting also for long-term drift, parasitic electromotive forces, and multimeter calibration.

Additionally, five Negative Temperature Coefficient (NTC) thermistors are embedded in the fluid path: at the inlet, outlet, middle, and along the leftmost and rightmost channels of the test panel. This configuration allows for comprehensive spatial mapping of temperature distribution, revealing the possible presence of asymmetries or edge effects, validating the system's thermal equilibrium, and offering an average temperature reference for external water temperature conditioning that is representative of the mean panel temperature.

The NTC sensors, also connected to a  $6\frac{1}{2}$ -digit multimeter (model 2700, Keithley) via a scanner module, were calibrated by comparison with a Standard Platinum Resistance Thermometer (SPRT) in a thermostatic bath over the temperature range from  $10^\circ\text{C}$  to  $40^\circ\text{C}$ , at eight calibration points. The calibration was performed with an associated expanded uncertainty of  $0.05^\circ\text{C}$ , ensuring the traceability of the measurements to the National standards, in accordance with the International Temperature Scale of 1990 (ITS-90) [24].

Fig. 2A reports on the left the temperature measured by the 5 NTCs, while Fig. 2B shows the difference between inlet and outlet water temperature ( $\Delta T$ ) measured by thermopile during laboratory characterization (room temperature controlled at  $23^\circ\text{C}$ ). The water flow rate and the water inlet temperature were kept at  $30 \text{ L/h}$  and  $25^\circ\text{C}$ , respectively. The thermopile voltage and the electrical resistance of the

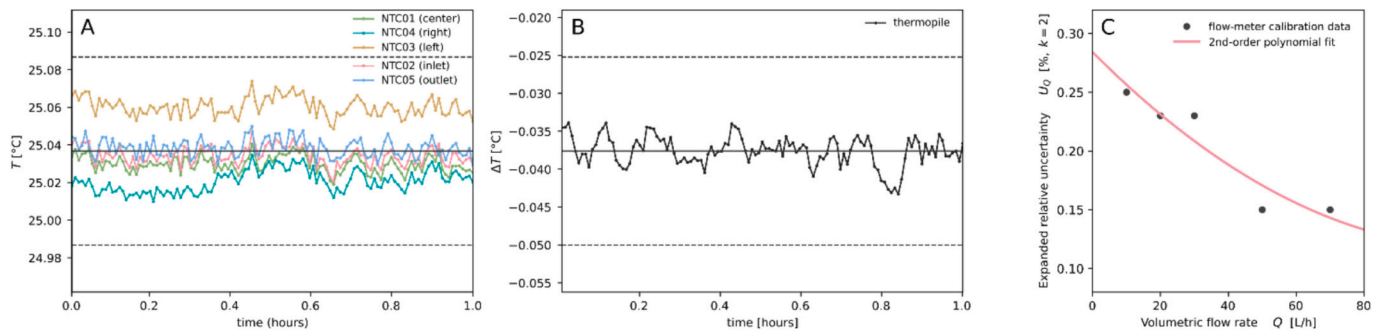


Fig. 2. Time series during laboratory characterization: (A) temperature measured by 5 NTCs, (B) inlet-outlet temperature difference ( $\Delta T$ ) measured by thermopile, shown within the adopted expanded uncertainty bands, and (C) water flux meter expanded relative uncertainty  $U_Q(Q)$  with a polynomial fit.

NTC thermistors were sampled every 30 s using the multimeter-scanner system and directly converted into temperature difference and temperature values using the calibrated thermopile sensitivity and the Steinhart–Hart equation, respectively. The resulting differences measured between each NTC are lower than calibration uncertainty evaluated equal to 0.05  $^{\circ}\text{C}$  (dashed in the figure).

### 2.3. Auxiliary radiative power estimation

Each channel houses a resistive heating wire, which can be activated under static conditions. In the absence of fluid motion (static mode) or under controlled flow, the net outgoing radiation flux leads to a measurable temperature decrease in the fluid. By activating the embedded heater and supplying power sufficient to maintain the aluminium plate at ambient temperature, the required electrical power input can provide an alternative evaluation of the radiative power loss. This provides a secondary, independent method for quantifying radiative power.

The idea of including two measurement methods in the same apparatus has a series of objectives:

- identify systematic biases affecting the electric heating method compared to the calorimetric approach;
- compare the two measurement methods in the same experimental conditions;
- validate the methods, establishing their performance characteristics and limitations of and verifying that they are fit for purpose.

### 2.4. Performance considerations

The experimental setup involves three simultaneous heat exchange processes: conduction, convection, and radiation. For accurate characterization of PRC materials, the influence of conduction and convection must be minimized, as our primary interest lies in radiative heat exchange. More in general, however, the apparatus allows to calculate the combined heat exchanges taking place for arbitrary input water temperature levels.

Several experimental strategies are employed in the setup to minimize parasitic heat flows and improve the system response. The emitting surface has been sized in such a way to maintain a manageable prototype while allowing sufficient area to generate a measurable water temperature difference between the inlet and outlet.

The fluid volume under the panel has been minimized to improve the system's response under transient conditions. The liquid content under the panel is about 0.67 L (equivalent to 2.7 L/m<sup>2</sup>). The water mass flow rate is another important parameter to consider, as it determines the residence time of water under the sample. A longer residence time allows for greater thermal exchange. As such, this parameter has been carefully tuned in previous studies involving liquid-cooling panels [20–22]: at high flow rates, temperature variations are smaller and more

difficult to detect. On the contrary, at low flow rates the thermal inertia of the system increases, as well as its susceptibility to non-radiative parasitics. Hence, a trade-off must be found aiming to maximize measurement accuracy and system responsiveness. The typical flow rates used in this study, 30 L/h corresponds to a complete renewal every 85 s, or about 5 min at 8 L/h.

The choice of construction materials (PMMA and EPS) and their thickness was driven by the need to achieve high thermal insulation and to limit conductive heat exchange with the environment. This is an important difference in how the two common measurement approaches to measure cooling fluxes respond to imperfect insulation: calorimetric methods tend to be conservative if insulation is insufficient (parasitic heat gains reduce the measured cooling flux), whereas Joule-heating methods are prone to overestimation if lateral heat leakage is not carefully controlled.

In terms of limitations, the apparatus is not intended for fully autonomous or off-grid deployment, as its operation requires a circulation pump and auxiliary temperature control, which presently rely on external power. In addition, the minimum panel size of 0.5 × 0.5 m<sup>2</sup> constrains testing to PRC materials that can be fabricated or applied at this scale, which may exclude early-stage materials available only in smaller formats. Finally, compared to compact electric-heater-based test rigs, the calorimetric design exhibits a larger thermal inertia due to the presence of a circulating working fluid. This results in a slower response to rapid environmental fluctuations, which may limit the characterization of fast transient effects but, conversely, can be advantageous for reducing measurement noise and enhancing stability under steady or quasi-steady conditions.

## 3. Uncertainty analysis

The estimation of individual uncertainties components and their combined impact on the overall measurement system are critical for validating design specifications and optimizing operational parameters, particularly in the context of differential temperature measurement.

In the evaluation of cooling power density uncertainty ( $U_q$ ), it is possible to separate two principal contributions, determined by the nominal uncertainty of the measurement sensors (subsection 3.1) and by the additional interaction with a non-radiative interference term (subsection 3.2).

### 3.1. Measurement sensors uncertainty

This section addresses the sensor-related contribution to the overall uncertainty budget of the proposed prototype. The analysis focuses on two dominant terms, namely the uncertainty associated with the temperature difference measurement and water flow rate.

Uncertainties are propagated, assuming independence of the dominant terms and neglecting uncertainty in  $c_p$ ,  $\rho$  (estimated to be of the order of 0.03%/°C), and  $A$ . With  $q = q(\Delta T, \dot{m})$ , the relative expanded

uncertainty is approximated by

$$\left(\frac{U_q}{q}\right)^2 \approx \left(\frac{U_{\Delta T}}{\Delta T}\right)^2 + \left(\frac{U_{\dot{m}}}{\dot{m}}\right)^2$$

and the absolute expanded uncertainty is

$$U_{\text{meas}}(q, Q) = q \sqrt{\left(\frac{U_{\Delta T}}{\Delta T(q, Q)}\right)^2 + \left(\frac{U_{\dot{m}}}{\dot{m}}\right)^2}$$

Since  $\dot{m} \propto Q$ , we set  $U_{\dot{m}}/\dot{m} \approx U_Q/Q$ .

The flow meter's relative calibration uncertainty ( $U_Q/Q$ ) was evaluated from the calibration data. The calibration function (Fig. 2C) is represented by a 2nd-order polynomial fit to the measured expanded uncertainty. Given the low uncertainty achieved across a wide range of fluxes, we expect the measurement-related uncertainty to be  $\Delta T$ -limited rather than  $Q$ -limited, as is often the case also with many examples presented in the literature [5,20,22,25].

As previously mentioned, the thermopile allows a direct measurement of  $\Delta T$  between inlet and outlet water temperature with an expanded uncertainty ( $k = 2$ ) equal to  $U_{\Delta T} = 12.4$  mK.

On the other hand, when using discrete temperature sensors to evaluate a temperature difference between the inlet and outlet (as commonly done in the literature), one should account for a critical increase in uncertainty. In fact, due to the difference operation, the uncertainty is propagated using the root sum of squares method for independent variables:

$$U_{\Delta T} = \sqrt{U_T^2 + U_T^2} = \sqrt{2}U_T$$

This calculation results in a combined absolute expanded ( $k = 2$ ) uncertainty of  $0.071$  °C for the temperature difference in case of the calibrated NTCs used in this study and other similar ones. In this condition, when  $\Delta T$  becomes small, an uncertainty of  $0.071$  °C for thermistors translates into a disproportionately large relative uncertainty. Assuming a desired target uncertainty of 10% on the determination of  $q$ , this value cannot be met unless the measured temperature difference is greater than  $0.71$  °C. Conversely, using a multi-thermocouple solution effectively meets the accuracy target across nearly its entire operational range, representing a significant improvement over conventional approaches.

Another significant practical advantage of the multi-thermocouple solution is its ability to achieve the desired level of accuracy even without the need for calibration of the multi-thermocouple. This stems from the common-mode rejection capabilities of differential measurements. In a differential measurement setup, the primary interest is the difference between two values, therefore, common-mode errors (e.g., uniform temperature shifts affecting both junctions equally) are inherently rejected. This means that the absolute accuracy of individual junctions is less critical than their relative consistency and stability, which are often easier to maintain without full calibration.

### 3.2. Non-radiative interference uncertainty term

This section addresses the additional contribution to the uncertainty budget arising from non-radiative heat transfer interference, which is not directly related to the measurement sensors but to rather to the thermal interaction between the panel and the surrounding environment.

In real application conditions, low measurement uncertainty alone is insufficient: when  $\Delta T$  becomes large (e.g., large area  $A$  at low  $Q$ ), the panel deviates farther from ambient, making convective/conductive parasitics terms more influential.

In order to quantify this effect, we introduce a lumped non-radiative magnitude.

$$U_{\text{nonrad}} = h_{\text{nonrad}} \Delta T_{\text{res}}$$

where  $h_{\text{nonrad}}$  ( $\text{W m}^{-2} \text{K}^{-1}$ ) is an effective coefficient, and  $\Delta T_{\text{res}}$  is an approximation for the typical panel-ambient temperature offset:

$$\Delta T_{\text{res}} \approx \alpha \Delta T.$$

With inlet temperature tracking (common in literature), a roughly linear temperature profile indicates a typical offset magnitude  $\Delta T_{\text{res}} \approx \Delta T/2$ , suggesting the use of a weighting  $\alpha = 0.5$ . With the midpoint tracking strategy (average value among the 5 NTC sensors positioned along the water channels) adopted in this work, the typical magnitude is reduced to  $\Delta T/4$ , hence  $\alpha = 0.25$ .

The effective uncertainty becomes

$$U_{\text{eff}} = \sqrt{U_{\text{meas}}^2 + U_{\text{nonrad}}^2}$$

Fig. 3 shows a study of the total expanded uncertainty as a function of net radiative power  $q$  (proportional to the measured  $\Delta T$ ) and flow rates. The left panels (A, C) consider only measurement sensor uncertainty, while the right ones (B, D) also include the non-radiative interference terms.

In the upper panels, the locus of points with minimal uncertainty is plotted over the scanned  $Q$ -range. In the measurement-only panel A, the red curve collapses to the lower  $Q$  boundary because  $U_{\Delta T}/\Delta T \propto 1/\Delta T$  favors larger  $\Delta T$ , i.e., lower  $Q$ . This is the typical situation where uncertainty is dominated by  $U_{\Delta T}/\Delta T(q, Q)$  rather than  $U_Q/Q$ . When this happens, the locus is uninformative. The situation is different when accounting for the presence of non-radiative parasitics, which we evaluate in Fig. 3B for a value of  $h_{\text{nonrad}} = 10 \text{ W m}^{-2} \text{K}^{-1}$ , typical for realistic application scenarios. In this case, we see that the uncertainty rises sharply at low flow rates, even though a relative uncertainty better than 10% is still achievable across a large parameter space of flow rates and cooling powers typical of PRC performance assessment experiments.

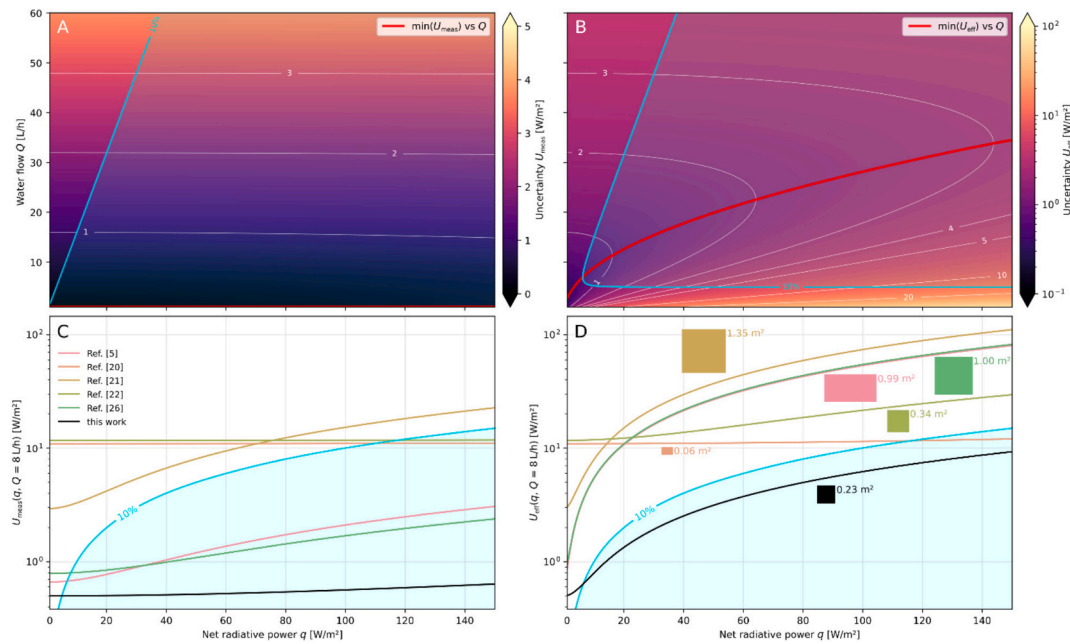
It is interesting to compare the expected uncertainty for similar calorimetric setups presented in the literature under typical fixed flow rate conditions used in the literature.

Table 1 summarizes geometric parameters and uncertainty values reported in previous literature studies. Unless the original paper explicitly states a coverage factor, reported accuracy values are treated as expanded uncertainties ( $k = 2$ ) to enable consistent comparison. The full uncertainty analysis and literature comparison is provided as an editable notebook, allowing key parameters (e.g., flow rate or non-radiative heat transfer coefficient) to be adapted to alternative operating conditions or hypothetical test configurations.

Fig. 3 C, D show the estimated uncertainties  $U_{\text{meas}}(q)$  and  $U_{\text{eff}}(q)$  including measurement-only factors and non-radiative interference, respectively, for a representative value of  $Q = 8$  L/h.

When comparing with other calorimetric setups, we see that some large-area configurations show relatively low uncertainty values in the measurement-only map because  $\Delta T$  scales with  $A$  [5,25]. However, once parasitics are taken into account, the same large  $\Delta T$  implies larger panel-ambient offsets and thus a larger non-radiative interference. By contrast, our proposed setup couples: (i) a compact area and therefore smaller offsets for a given operating point, (ii) a direct differential thermopile  $\Delta T$  measurement with low  $U_{\Delta T}$ , and (iii) midpoint tracking (smaller  $\alpha$ ), which jointly sustain low uncertainty across a broad  $q$ -range even for realistic parasitic heat transfer contributions.

Thanks to the calibrated water flow meter and differential thermopile measurement, the proposed prototype reaches the lowest uncertainty across all values of radiative fluxes, even when compared to larger-area devices, providing a realistic lower bound for the minimum uncertainty attainable with this class of setups. When accounting for a representative non-radiative contribution of  $h_{\text{nonrad}} = 10 \text{ W m}^{-2} \text{K}^{-1}$ , the compact form factor of the setup allows to keep a more homogeneous temperature and smaller temperature drop across the emitting surface, which limits the influence of non-radiative parasitics. This allows sub-10% relative uncertainty measurements across almost the whole range of  $q$  values typical of radiative cooling materials.



**Fig. 3.** Absolute uncertainty maps for the proposed setup. Panels (A, C) consider only measurement sensor uncertainty, while panels (B, D) also include the non-radiative interference term with a representative coefficient  $h_{\text{nonrad}} = 10 \text{ W m}^{-2} \text{ K}^{-1}$ . The cyan contour and shaded area indicate the region where the relative uncertainty remains below 10%. The red curves in panels (A, B) indicate the locus of  $(q, Q)$  values corresponding to the minimum absolute uncertainty. Lower panels (C, D) include a comparison with other experimental setups in the literature, at a typical flow value of  $Q = 8 \text{ L/h}$ . Each curve is labelled with the emitting surface area of the panel. (For interpretation of the references to colour in this figure legend, the reader is referred to the web version of this article.)

**Table 1**  
Uncertainty comparison against literature data.

Ref	$A$ ( $\text{m}^2$ )	$\alpha$	Meas. method	$U_T$ (K)	$U_{\Delta T}$ (K)	$U_Q$
[5]	0.9936	0.5	2 sensors	0.05	0.071	2%
[20]	0.06	0.5	2 sensors	0.05	0.071	1%
[21]	1.3456	0.5	2 sensors	0.30	0.42	1.2 L/h
[22]	0.3364	0.5	2 sensors	0.30	0.42	1%
[25]	1.00	0.5	2 sensors	0.06	0.085	1.5%
This work	0.23	0.25	direct $\Delta T$	—/—	0.012	< 0.28%

#### 4. Conclusions

The experimental setup presented in this study constitutes a robust and high-precision tool for the metrological evaluation and comparison of passive radiative cooling materials. By combining calorimetric principles with a tailored structural design and accurate thermal measurements, the apparatus enables quantitative characterization of PRC materials with good confidence.

Compared with experimental setups and methods currently described in the literature, the proposed apparatus offers several advantages. Its design is based on a rigorous metrological approach, ensuring that all employed instruments and sensors are calibrated against National standards and that all measured quantities are associated with a clearly defined uncertainty budget traceable to SI standard. The adopted design choices and sensor selection minimize measurement uncertainty and improve the reliability and reproducibility of the results.

Notably, the uncertainty analysis reveals the existence of a practical lower bound that affects radiative cooling power density measurements. This bound arises from intrinsic technical and design constraints and is already significant even when additional uncertainty contributions—such as those associated with outdoor deployment and environmental variability—are neglected. The analysis further indicates that achieving relative uncertainties on the order of 10% is non-trivial and requires careful consideration of sensor selection, calibration,

geometry and operating conditions during the experimental design phase.

The apparatus allows the cooling power of PRC materials to be evaluated using two independent approaches: calorimetric determination based on the inlet–outlet temperature difference of a flowing liquid, and electrical power compensation under static or controlled conditions. The possibility of applying and comparing these two methods within the same experimental platform provides a valuable means to identify systematic biases and assess the limitations of each approach. This type of implementation is also highly relevant to real-world applications, where passive radiative cooling technologies are expected to operate predominantly through heat-transfer fluids. In this context, the proposed setup enables assessment of cooling power under realistic thermal loads and facilitates the identification of operating conditions that optimize the combined effect of water flow rate and temperature difference.

Future work will focus on in-field measurement campaigns using reference PRC materials with well-characterized thermo-physical properties. More broadly, we hope that the strategies discussed in this paper to optimize different measurement aspects will encourage the scientific community to devote greater attention to the metrological aspects of radiative cooling measurements, and their uncertainty evaluation.

#### CRedit authorship contribution statement

**G. Lopardo:** Writing – review & editing, Writing – original draft, Conceptualization. **F. Bertiglia:** Visualization, Data curation. **G. Braccialarghe:** Investigation. **M. Florio:** Investigation. **F. Girard:** Writing – original draft, Methodology. **D. Giraudi:** Investigation. **F. Santoro:** Investigation. **L. Pattelli:** Writing – review & editing, Funding acquisition.

#### Declaration of competing interest

The authors declare that they have no known competing financial interests or personal relationships that could have appeared to influence

the work reported in this paper.

## Acknowledgments

This work was supported by the European project PaRaMetriC, code 21GRD03. The project 21GRD03 PaRaMetriC received funding from the European Partnership on Metrology, cofinanced by the European Union's Horizon Europe Research and Innovation Programme and from the Participating States.

## Data availability

The data and uncertainty analysis scripts used in this work are available at: <https://doi.org/10.5281/zenodo.18504044>.

## References

- [1] J. Kennedy, State of the global climate 2024, WMO, 2025, 1368, <https://library.wmo.int/idurl/4/69455>.
- [2] J. Tollefson, Earth breaches 1.5°C climate limit for the first time: what does it mean? *Nature* 637 (2025) 769–770, <https://doi.org/10.1038/d41586-025-00010-9>.
- [3] X. Lim, The super-cool materials that send heat to space, *Nature* 577 (2020) 18–20, <https://doi.org/10.1038/d41586-019-03911-8>.
- [4] H. Li, J. Zhao, M. Li, S. Deng, Q. An, F. Wang, Performance analysis of passive cooling for photovoltaic modules and estimation of energy-saving potential, *Solar Energy* 181 (2019) 70–82, <https://doi.org/10.1016/j.solener.2019.01.014>.
- [5] B. Zhao, M. Hu, X. Ao, N. Chen, Q. Xuan, D. Jiao, G. Pei, Performance analysis of a hybrid system combining photovoltaic and nighttime radiative cooling, *Appl. Energy*, Volume 252, 2019, 113432, ISSN 0306-2619, doi:<https://doi.org/10.1016/j.apenergy.2019.113432>.
- [6] A. Baniassadi, D.J. Sailor, G.A. Ban-Weiss, Potential energy and climate benefits of super-cool materials as a rooftop strategy, *Urban Clim.* 29 (2019) 100495, <https://doi.org/10.1016/j.uclim.2019.100495>.
- [7] J. Chen, L. Lin, Comprehensive evaluation of thermal and energy performance of radiative roof cooling in buildings, *J. Build. Eng.* 33 (2021) 101631, <https://doi.org/10.1016/j.jobbe.2020.101631>.
- [8] Y. Peng, J. Chen, A. Y. Song, A.Y., P. B. Catrysse, P. C. Hsu, L. Cai, B. Liu, Y. Zhu, G. Zhou, D. S. Wu, H. R. Lee, S. Fan, Y. Cui, Nanoporous polyethylene microfibrils for large-scale radiative cooling fabric. *Nat. Sustain.* 1, 105–112 (2018). doi:<https://doi.org/10.1038/s41893-018-0023-2>.
- [9] P.C. Hsu, A.Y. Song, P.B. Catrysse, C. Li, Radiative human body cooling by nanoporous polyethylene textile, *Science* 353 (2016) 1019–1023.
- [10] D. Forte, C. Belotti, L. Pattelli, M. Morciano, E. Chiavazzo, P. Asinari, M. Fasano, Modeling of daytime radiative cooling enhanced vapor-compression refrigeration systems, *Energy* 340 (2025) 139101, <https://doi.org/10.1016/j.energy.2025.139101>.
- [11] S. Yoon, M. Kim, J. Seo, S. Kim, H. Lee, J. Lee, B.J. Lee, Performance analysis of a hybrid HVAC system consisting of a solar thermal collector and a radiative cooling panel, *Energ. Buildings* 241 (2021) 110921, <https://doi.org/10.1016/j.enbuild.2021.110921>.
- [12] M. Zeyghami, F. Khalili, Performance improvement of dry cooled advanced concentrating solar power plants using daytime radiative cooling, *Energ. Convers. Manage.* 106 (2015) 10–20.
- [13] A.K. Stark, A.J.F. Klausner, An R&D strategy to decouple energy from water, *Joule* 1 (3) (2017) 416–420, <https://doi.org/10.1016/j.joule.2017.10.009>.
- [14] D. Tichý, L. Pattelli, C. Efthymiou, Margarita-Niki Assimakopoulos, M. Voldán, Figures of merit of passive daytime radiative cooling materials, EPJ Web of Conferences, 2025, 323, 10001, doi:<https://doi.org/10.1051/epjconf/202532310001>.
- [15] F. Fan, D. Xu, Y. Zhu, G. Tan, D. Zhao, A simple, accurate, and universal method for characterizing and comparing radiative cooling materials and devices, *Int. J. Heat Mass Transf.* 200 (2023) 123494, <https://doi.org/10.1016/j.ijheatmasstransfer.2022.123494>.
- [16] J. Qin, Z. Zhang, Y. Li, Y. Cai, H. Zhang, L. Liu, L. Xu, W. Zhang, Xi. Xue, Design and manufacture of a radiative cooler to measure the subambient cooling effect and cooling power, *Rev. Sci. Instrum.* 93 (2022) 054901, <https://doi.org/10.1063/5.0087494>.
- [17] C. Sui, Po-Chun Hsu, Standardizing the thermodynamic definition of daytime subambient radiative cooling, *ACS Energy Lett.*, 2024, 9, 6, 2997–3000, <https://pubs.acs.org/doi/https://doi.org/10.1021/acsenerylett.4c00909>.
- [18] K. Bu, X. Huang, X. Li, H. Bao, Consistent assessment of the cooling performance of radiative cooling materials, *Adv. Funct. Mater.* 33 (2023) 2307191, <https://doi.org/10.1002/adfm.202307191>.
- [19] L. Zhou, X. Yin, Q. Gan, Best practices for radiative cooling, *Nat. Sustainability* 6 (2023) 1030–1032, <https://doi.org/10.1038/s41893-023-01170-0>.
- [20] L. Jia, L. Lu, Q. Gong, K. Jiao, Analytical and experimental analyses on cooling performances of radiative SkyCool radiators with various interior flowing channels, *Energy* 295 (2024) 130907. ISSN 0360-5442, <https://doi.org/10.1016/j.energy.2024.130907>.
- [21] A. Aili, D. Zhao, J. Lu, Y. Zhai, X. Yin, G. Tan, R. Yang, A kW-scale, 24-hour continuously operational, radiative sky cooling system: experimental demonstration and predictive modeling, *Energy Convers. Manage.*, 2019, 186, 586–596, ISSN 0196-8904, doi:<https://doi.org/10.1016/j.enconman.2019.03.006>.
- [22] E. Goldstein, A. Raman, S. Fan, Sub-ambient non-evaporative fluid cooling with the sky, *Nat. Energy* 2 (2017) 17143, <https://doi.org/10.1038/nenergy.2017.143>.
- [23] A.P. Raman, M.A. Anoma, L. Zhu, E. Rephaeli, S. Fan, Passive radiative cooling below ambient air temperature under direct sunlight, *Nature* 515 (2014) 540–544, <https://doi.org/10.1038/nature13883>.
- [24] H. Preston-Thomas, The international temperature scale of 1990 (ITS-90), *Metrologia* 27 (3) (1990). <https://iopscience.iop.org/article/10.1088/0026-1394/27/1/002/pdf>.
- [25] F. Wang, J. Guo, Y. Liu, W. Zheng, Y. Jiang, C. Sun, Comparative experimental study on integrated radiative and evaporative cooling: performance and economic benefits, *Energ. Convers. Manage.* 352 (2026) 121062.